Available online at www.sciencedirect.com

ScienceDirect

Geochimica et Cosmochimica Acta 245 (2019) 172–189

Geochimica et Cosmochimica Acta

www.elsevier.com/locate/gca

The clumped ($^{13}C—^{18}O$) isotope composition of echinoid calcite: Further evidence for "vital effects" in the clumped isotope proxy

Amelia J. Davies *, Cédric M. John

Department of Earth Science and Engineering, Imperial College London, UK

Received 31 January 2018; accepted in revised form 27 July 2018; available online 13 August 2018

Abstract

Carbonate clumped isotope thermometry is based on the thermodynamically dependent relative abundance of $^{13}C—^{18}O$ bonds (quantified as Δ_{47}) within the carbonate crystal lattice. The clumping of $^{13}C—^{18}O$ in carbonates is based on a self-reaction of isotope exchange that occurs rapidly at near neutral pH. Similar Δ_{47}-temperature relationships between biogenic and inorganically precipitated carbonate in initial studies led to the promise of a proxy free of biologically driven disequilibrium effects, commonly referred to as "vital effects". This has been largely the case for most organisms investigated. Biologically mediated disequilibrium precipitation has however been reported in corals and cephalopods and brachiopod molluscs. Echinoderms, despite their complex inter-cellular bio-mineralization strategy, large inter-skeletal fractionation of $\delta^{18}O$, $\delta^{13}C$ and rapid calcite precipitation have however not been previously investigated with regards to their clumped isotope composition. We present clumped isotopic composition (Δ_{47}) of 25 inter-skeletal elements of 5 echinoid species with varying growth temperatures. We found no statistically significant inter-skeletal variation in Δ_{47} in all echinoid species measured, a surprising find given the important inter-skeletal variability reported for $\delta^{13}C$ and $\delta^{18}O$. Our echinoid Δ_{47}-temperature calibration however shows a statistically significant positive offset from Δ_{47}-temperature calibration for inorganic calcite of 0.014‰. The pattern of isotopic fractionation in $\delta^{18}O$ and Δ_{47} of echinoderms is not consistent with CO_2 hydration or hydroxylation, diffusion or the high-Mg calcite composition of echinoid calcite. Positive offsets in the Δ_{47} of echinoid calcite may however relate to deviations in the pH of the calcifying fluid from the pH at which equilibrium calcite is precipitated.

Keywords: Clumped isotope; Echinoids

1. INTRODUCTION

Measurement of the ratio of stable oxygen isotopes $^{16}O/^{18}O$ in biogenic carbonate is a well-established proxy for quantitative paleoclimate reconstruction (Urey, 1947; Epstein et al., 1951; Emiliani, 1955). This technique is however based on an *a priori* assumption of the $\delta^{18}O$ of seawater, which can vary both geographically and through time. Furthermore, while the stable oxygen isotopic composition of some taxa faithfully reflects both the temperature and the $\delta^{18}O$ of seawater, other taxa show specific discrepancies known as "vital effects" (Epstein et al., 1951).

Carbonate clumped isotope thermometry is a temperature based proxy examining the thermodynamically dependent "clumping" of ^{13}C and ^{18}O within the carbonate crystal lattice (Eiler and Schauble, 2004; Ghosh et al., 2006; Eiler, 2007). This is based on the homogeneous isotope exchange equilibrium $M^{13}C^{16}O_3 + M^{12}C^{18}O^{16}O_2 \rightleftharpoons M^{13}C^{18}O^{16}O_2 + M^{12}C^{16}O_3$ (where M is a metal such as Ca), a system that undergoes rapid oxygen isotope

* Corresponding author.
E-mail address: ad5209@ic.ac.uk (A.J. Davies).

https://doi.org/10.1016/j.gca.2018.07.038
0016-7037/

exchange at a near neutral pH. At low temperatures the formation of $^{13}C—^{18}O$ bonds is promoted as the vibrational energy in a heavy-heavy bond is less than half that of the corresponding light–light bond. Decreasing temperature thus favors the formation of $M^{13}C^{18}O^{16}O_2$ (Schauble et al., 2006). The excess of $^{13}C^{18}O^{16}O$ relative to a stochastic distribution, in which all isotopes are equally distributed among isotopologues, is then measured and expressed using the metric Δ_{47} defined as:

$$\Delta_{47} = \left[\left(\frac{R^{47}}{R^{47*}} - 1\right) - \left(\frac{R^{46}}{R^{46*}} - 1\right) - \left(\frac{R^{45}}{R^{45*}} - 1\right)\right] \times 1000 \quad (1)$$

where $Ri = mi/m44$ and R^* gives the abundance of each isotopolgue of a gas with the same bulk isotopic composition as R but with a stochastic distribution (Affek and Eiler, 2006). As this is a self-reaction of isotope exchange, the estimate for the carbonate formation temperature is independent of the oxygen isotopic composition of the parent fluid (Eiler, 2007). This is particularly useful in climate reconstruction where determination of the temperature and $\delta^{18}O$ composition of water is important in discerning other environmental factors such as geographic distribution of ice, ocean circulation, and the hydrological cycle (Eiler, 2011).

The term "vital effects" refers to the offset between the isotopic compositions of biogenic carbonates and inorganic carbonates precipitated under identical conditions. The success of the clumped isotope thermometer has a strong basis in the congruence between empirical calibrations using biogenic carbonates (Ghosh et al., 2006; Ghosh et al., 2007; Came et al., 2007; Eagle et al., 2010) and calibrations based on inorganic precipitation experiments (Ghosh et al., 2006; Dennis and Schrag, 2010). In particular groups that show significant non-equilibrium fractionation of $\delta^{18}O$ and $\delta^{13}C$ appear free of vital effects in their clumped isotopic composition (Tripati et al., 2010; Thiagarajan et al., 2011; Grauel et al., 2013; Katz et al., 2017). Furthermore empirical calibrations are in good accordance with theoretical calculations of isotopic clumping on varying temperature (Schauble et al., 2006; Guo et al., 2009).

Subtle non-equilibrium fractionations in the clumped isotope composition of shallow warm-water corals (Saenger et al., 2012), deep-sea cold-water corals (Thiagarajan et al., 2011; Spooner et al., 2016), cephalopods (Dennis et al., 2013) and molluscs (Henkes et al., 2013) have however been reported. Deviations from equilibrium precipitation, as defined by inorganic precipitation experiments, are group dependent and tend to both higher and lower Δ_{47} (Passey and Henkes, 2012; Saenger et al., 2012; Dennis et al., 2013; Henkes et al., 2013; Kimball et al., 2015). The drivers of group specific non-equilibrium fractionations however remain elusive and are complicated by uncertainties in how well inorganic calibrations reflect true equilibrium values (Zaarur et al., 2013).

Improvements in data processing for clumped isotope analysis (Daëron et al., 2016; Schauer et al., 2016) in association with comprehensive inorganic calibration of the thermometer over a wide temperature range and steps towards the development of a "universal temperature-Δ_{47} calibration" (Kluge et al., 2015; Bonifacie et al., 2016; Kelson et al., 2017) have reduced uncertainties in the true slope and intercept of the inorganic Δ_{47}-temperature relationship. It is therefore now easier to assess non-equilibrium fraction in the clumped isotope composition of biogenic carbonate, notably in groups that show a strong disequilibrium signal in $\delta^{18}O$ and $\delta^{13}C$.

One such group is echinoderms. The stable isotopic composition of echinoid skeletal elements has been well characterised (Weber and Raup, 1966a; Weber and Raup, 1966b; Weber, 1968; Courtney and Ries, 2015). Inter-skeletal elements differ by several parts per thousand in $\delta^{18}O$ and $\delta^{13}C$ with enrichment of $\delta^{13}C$ of up to 12‰ in test calcite in comparison with spines. $\delta^{18}O$ fractionation in echinoid spines is inversely related to temperature while $\delta^{13}C$ in spines is positively correlated with atmospheric pCO_2. Echinoids are capable of rapid calcification (Gorzelak et al., 2011). $\delta^{18}O$ and $\delta^{13}C$ e also correlate with calcification rate (Courtney and Ries, 2015). Correcting for the effects of growth temperature, atmospheric pCO2 and calcification rate on $\delta^{18}O$ and $\delta^{13}C$ fractionation $\delta^{18}O$ and $\delta^{13}C$ remain positively correlated indicating the presence of unaccounted for vital effects (Courtney and Ries, 2015).

Echinoids have a unique strategy of intercellular biomineralization, depositing high magnesium calcite (Chave, 1954; Schroeder et al., 1969; McClintock et al., 2011) on an organic matrix to generate a three-dimensional mesh known as a stereom with an initial phase of ACC deposition (Markel et al., 1986). Demonstrated links between calcification rate and vital effects in stable $\delta^{18}O$ and $\delta^{13}C$ isotopic composition, unique biomineralization strategy and large magnitude of isotopic fractionation, especially in $\delta^{13}C$, make the echinoids an excellent group in which to test for "vital effects" in clumped isotope composition.

Here we present the first systematic measurements of the clumped isotopic composition (Δ_{47}) of modern echinoderm calcite. This study both adds to existing biogenic calibration of the clumped isotope analysis and adds to our understanding of vital effects acting upon the clumped isotope composition of calcite.

2. METHODOLOGY

2.1. Samples

Echinoid samples were collected at four different localities around the globe mostly live from the benthos with one specimen grown by aquaculture (Table 1). Live collection of specimens enables us to discount post-mortem mineralogical alteration from high-Mg calcite. It also minimises the potential for post-mortem isotopic alteration in the littoral zone, either by marine or meteoric digenesis. Echinoid species *Diadema Setosum* and *Tripneustes Gratilla* were fished in Indonesian waters and transported live to Imperial College where they were maintained in an aquarium at 25℃. Echinoid species *Paracentrotus Lividus* were collected live at 1.5 m depth in the eastern Mediterranean. Deceased irregular echinoids *Dendraster Excentricus* were sampled from the foreshore at Morro Bay on the Pacific coast,

Table 1
Specimen sampling details and collection location. Growth water temperature and stable oxygen isotopic composition of analysed samples.

Sample Information					Seawater properties	
Sample name	Order	Genus	Inter-skeletal element	Location	Temperature (℃)[a]	δ^{18}Owater VSMOW (‰)[b]
GA1	*Temnopleuroida*	*Tripneustes*	Ambulacral Column	Indonesia, Java Sea	28.4 ± 0.15	0.28 ± 0.02
GA2	*Temnopleuroida*	*Tripneustes*	Interambulacral Column	Indonesia, Java Sea	27.8 ± 0.15	0.28 ± 0.02
GLT	*Temnopleuroida*	*Tripneustes*	Tooth	Indonesia, Java Sea	27.8 ± 0.15	0.28 ± 0.02
GS	*Temnopleuroida*	*Tripneustes*	Spine	Indonesia, Java Sea	27.8 ± 0.15	0.28 ± 0.02
GT	*Temnopleuroida*	*Tripneustes*	Bulk Test	Indonesia, Java Sea	27.8 ± 0.15	0.28 ± 0.02
BS	*Diadematoida*	*Diadema sp.*	Spine	Indonesia, Java Sea	27.8 ± 0.15	0.28 ± 0.02
BT	*Diadematoida*	*Diadema sp.*	Bulk Test	Indonesia, Java Sea	27.8 ± 0.15	0.28 ± 0.02
MA1	*Clypeasteroida*	*Dendraster*	Ambulacral Column	Morro Bay, CA	13.4 ± 0.03	−0.57 ± 0.03
MA2	*Clypeasteroida*	*Dendraster*	Interambulacral Column	Morro Bay, CA	13.4 ± 0.03	−0.57 ± 0.03
MB	*Clypeasteroida*	*Dendraster*	Base of test	Morro Bay, CA	13.4 ± 0.03	−0.57 ± 0.03
ML	*Clypeasteroida*	*Dendraster*	Lantern (teeth, pyramid, rotula)	Morro Bay, CA	13.4 ± 0.03	−0.57 ± 0.03
MP	*Clypeasteroida*	*Dendraster*	Petal	Morro Bay, CA	13.4 ± 0.03	−0.57 ± 0.03
MS	*Clypeasteroida*	*Dendraster*	Spine	Morro Bay, CA	13.4 ± 0.03	−0.57 ± 0.03
YA1	*Camarodonta*	*Paracentrotus*	Ambulacral Column	San Andrea, Elba, IT	18.5 ± 0.54	1.36 ± 0.03
YA2	*Camarodonta*	*Paracentrotus*	Interambulacral Column	San Andrea, Elba, IT	18.5 ± 0.54	1.36 ± 0.03
YLP	*Camarodonta*	*Paracentrotus*	Pyramid	San Andrea, Elba, IT	18.5 ± 0.54	1.36 ± 0.03
YLR	*Camarodonta*	*Paracentrotus*	Rotula	San Andrea, Elba, IT	18.5 ± 0.54	1.36 ± 0.03
YLT	*Camarodonta*	*Paracentrotus*	Teeth	San Andrea, Elba, IT	18.5 ± 0.54	1.36 ± 0.03
YS	*Camarodonta*	*Paracentrotus*	Spine	San Andrea, Elba, IT	18.5 ± 0.54	1.36 ± 0.03
YT	*Camarodonta*	*Paracentrotus*	Bulk Test	San Andrea, Elba, IT	18.5 ± 0.54	1.36 ± 0.03
SDA1	*Strongylocentrotus*	*Droebachiensis*	Ambulacral Column	University of Maine	8.5 ± 0.2	−1.2 ± 0.009
SDA2	*Strongylocentrotus*	*Droebachiensis*	Interambulacral Column	University of Maine	8.5 ± 0.2	−1.2 ± 0.009
SDS	*Strongylocentrotus*	*Droebachiensis*	Spine	University of Maine	8.5 ± 0.2	−1.2 ± 0.009
SDLT	*Strongylocentrotus*	*Droebachiensis*	Tooth	University of Maine	8.5 ± 0.2	−1.2 ± 0.009
SDT	*Strongylocentrotus*	*Droebachiensis*	Bulk Test	University of Maine	8.5 ± 0.2	−1.2 ± 0.009

[a] Ocean temperature estimated from the NOAA World Ocean Atlas 2013 (v.2) (Locarnini et al., 2013). Standard error reflects difference in seasonal temperatures over the habitual depth range of groups listed

[b] Water δ^{18}O values estimated from the global gridded data set of oxygen isotope composition in water (LeGrande & Schmidt, 2006) excluding Strongylocentrotus Droebanchiensis where water δ^{18}O was directly measured from an aliquot taken from the aquaculture tank

USA. Only *Dendraster Excentricus* specimens with spines still attached and organic components still present were selected ensure selected specimens were recently deceased. *Stronglyocentrotus Droebachiensis,* hatched and grown in an aquaculture facility, were provided by the Centre for co-operative Aquaculture, University of Maine. Growth by aquaculture provides a very well constrained record of growth temperature over the lifespan of the echinoid. Echinoid samples were classified by order (Table 1) and are addressed as such in results and discussion sections for ease of referral.

Growth temperatures for samples collected from the benthos were estimated from the World Ocean Database (V.2) (Locarnini et al., 2013). over estimated specimen growth depth. This depth was 0–10 m for *Diadema Setosum* and *Tripneustes Gratilla* (Cleary et al., 2005; Ristanto et al., 2018) 0–5 m for *Dendraster Excentricus* (Merrill and Hobson, 1970) and 0–5 m as sampled for *Paracentrotus Lividus*. Average and standard deviation in annual seawater temperature at each collection location is taken from the World Ocean Database (V2) (Locarnini et al., 2013). The growth temperature of *Stronglyocentrotus Droebachiensis* is calculated from weekly temperature measurements within the aquarium over the course of specimen growth.

Seawater $\delta^{18}O$ values were estimated from the global gridded dataset of LeGrande and Schmidt (2006). Where possible values were assumed over the depth range of the species, otherwise sea surface measurements (0 m depth) are used. Database $\delta^{18}O_{sw}$ is converted into expected $\delta^{18}O_{carbonate}$ using the calibration of (Mavromatis et al., 2012). Expected $\delta^{18}O_{carbonate}$ VSMOW (‰) is then converted into $\delta^{18}O_{carbonate}$ VPDB (‰) using established equation $\delta^{18}O_{VPDB} = 0.97001(\delta^{18}O_{VMOW}) - 29.99$ (Coplen, 1988).

2.2. Stable isotopic measurements

We sampled echinoid inter-skeletal elements as illustrated in Fig. 1. Ambulacral regions such as those shaded red and interambulacral regions such as those shaded in yellow (Fig. 1) were powdered using a dental drill. Elements of the lantern were disarticulated, separated and powdered using a pestle and mortar. The longest spines were selected from the region of largest test diameter, removed and gently crushed with a pestle and mortar. We also took "bulk" test measurements consisting of over 3 cm^2 areas of test calcite composing both ambulacral and interambulacral regions which were separately crushed.

Isotopic analyses were carried out in the Qatar Stable Isotope Laboratory at Imperial College London. Typical sample sizes were in the range of 5–8 mg per replicate.

To remove organic contaminants all samples were treated by low temperature plasma ashing under oxygen at a flow rate of 400 ml/min power of 1000w with a treatment time of between 30 and 45 min. Lebeau et al. (2014) recommend low temperature ashing for measurement of stable $\delta^{13}C$ and $\delta^{18}O$ as it facilitates the removal of organic matter whilst preserving isotopic abundances. In order to ensure low temperature oxygen plasma ashing has not affected Δ47 of echinoid samples we treated carbonate standard ETH3 using the same technique. Δ47 of untreated ETH3 standard ($\mu = 0.71 \pm 0.015$, $n = 8$) is within range of plasma treated ETH3 standard measured at Imperial over the same measurement period ($\mu = 0.69 \pm 0.015$, $n = 8$). We can thus assume that positive offset in echinoid Δ47 from the inorganic calibration is not as a result of difference in analytical protocol. We see no significant effect on stable $\delta^{13}C$ and $\delta^{18}O$ of ETH3 on oxygen plasma ashing these being $\delta^{18}O_{VPDB} = -1.74$, $\delta^{13}C_{VPDB} = 1.70$ and being $\delta^{18}O_{VPDB} = -1.76$, $\delta^{13}C_{VPDB} = 1.69$ in non-treated and treated samples respectively.

The relative abundance of the $^{13}C^{18}O^{16}O$ isotoplogue in acid evolved carbon dioxide is directly proportional to the extent of $^{13}C{-}^{18}O$ ordering in the carbonate phase (Ghosh et al., 2006). Powdered samples are thus reacted individually in 105% orthophosphoric acid at 90 °C for 10 min following (McCrea, 1950) and (Swart et al., 1991). Evolved carbon dioxide was purified using a series of water traps and "static" Porapak -Q packed U-trap through which gas is transferred without helium flow using both the pull of liquid nitrogen and a pressure differential across the trap (Davies and John, 2017).

Analyte CO_2 was measured on dual inlet Thermo 253 mass spectrometer with faraday cups registered through m/z 44–49. The dual inlet system allows rapid repeated inter-comparison between sample and reference gas, a CO_2 standard from Oztech $\delta^{13}C_{VPDB}$ −3.64‰, $\delta^{18}O_{VSMOW}$ 25.01‰. Measurements comprised 8 acquisitions each with

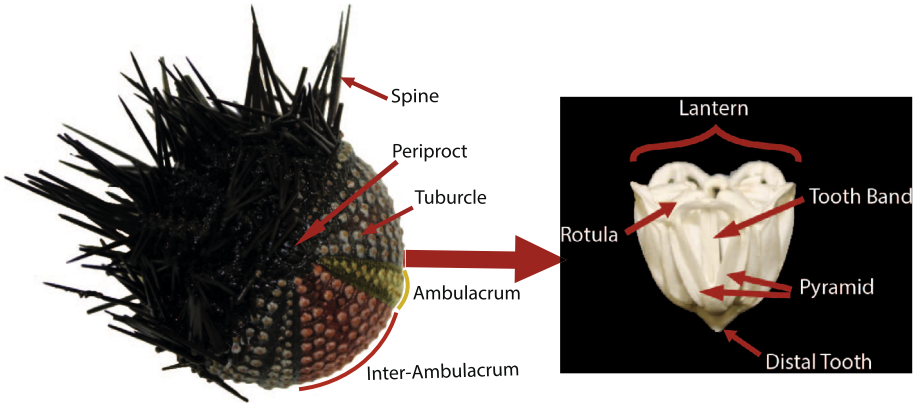

Fig. 1. Illustration of inter-skeletal elements sampled within echinoids. Echinoid pictured is *Paracentrotus Lividus.*

7 cycles with 26 s integration time. A typical acquisition time is 20 min corresponding to a total analysis time of 2.5–3 h. This measurement is repeated at least three times per sample.

2.3. Data analysis and reduction

The $^{13}C^{18}O^{16}O$ isotopologue constitutes approximately 97% of the abundance of CO_2 measured on mass 47 (Eiler, 2007). The isotopic parameters of (Brand et al., 2010) are used in calculation of raw Δ_{47}, as these have been shown to better account for anomalies in sample ^{17}O thus produce accurate Δ_{47} values independent of sample bulk isotopic composition (Daëron et al., 2016; Schauer et al., 2016). All calculations and corrections are carried out in the freely available stable isotope management software *Easotope* (John and Bowen, 2016).

Raw Δ_{47} is corrected in three steps. In order to correct for non-linearity of the mass spectrometer, heated gasses with different bulk isotopic compositions, were measured and normalized by projecting all Δ_{47} measurements to a δ47 of 0. Heated gasses were prepared following the procedure described by (Davies and John, 2017). Δ_{47} measurements corrected for non-linearity were then translated into the absolute reference frame of (Dennis et al., 2011). Carbonate standards routinely measured to allow for translation into the absolute reference frame are Carrara Marble, ETH2 and ETH3. Full details of the heated gas and carbonate standards run over the course of the measurement period can be found in the supplementary material (Annex 1). Δ_{47} is corrected for acid fractionation by adding the acid fractionation factor 0.082‰ (Defliese et al., 2015). $\delta^{18}O$ is corrected for phosphoric acid digestion at 90 °C using an acid fractionation factor of 1.0081‰ (Kim et al., 2007).

Supplementary data associated with this article can be found, in the online version, at https://doi.org/10.1016/j.gca.2018.07.038.

Masses 48 and 49 were used to detect the presence of contaminants. Samples with Δ_{48} offset values > 1.5‰ or 49 parameter values > 0.2 were excluded from analysis following Davies and John (2017).

2.4. Statistical methods

Statistical analysis was carried out using the software *JMP® version 13.2.0.* The appropriate application of statistical methods strengthens conclusions based on available data. The Δ_{47}, $\delta^{13}C$ and $\delta^{18}O$ values of homogenous carbonate standards (e.g. Carrara Marble n = 53, ETH3 n = 147) are normally distributed. Therefore, we assume normality in the distribution of our sample data (n = 3–4), allowing for the application of parametric statistical tests. Average standard deviation (σ) sample on Δ_{47} for 3–4 replicates is 0.0147‰.

One-way ANOVA (ANalysis Of VAriance) tests enable us to determine if data of sample size *N* from a given number groups *k* of equal or unequal size *n* have a common mean *m.* The null hypothesis assumes a common mean. It is a parametric test but robust to modest violations in sample normality. One way-ANOVA tests are reported following APA style (American Psychological Association, 1994). If the null hypothesis is rejected by one-way ANOVA we carry post-hoc pairwise student t-tests to confirm where difference occurs between groups. We then use effect size in association with group number, sample size and significance level to calculate statistical power using G*Power (Faul et al., 2007). Power values tells us the probability of detecting a "true" effect i.e. rejecting a false null hypothesis. Low power values indicate a smaller chance of rejecting a false null hypothesis. Further details of these calculations are included in Appendix 1.

ANCOVA (ANalysis Of COVAriance) tests are used to determine differences in Δ_{47}-temperature relationship between inorganic and biogenic calibrations. ANCOVA combines ANOVA and regression analysis enabling the user to determine if groups have a common mean *m*, whilst controlling for the effect of covariates. As with ANOVA we carry out carry post-hoc pairwise student t-tests to confirm where difference occurs between groups and use effect size in combination with sample size to calculate statistical power at a significance level of 0.05 (Table 4).

3. RESULTS

The isotopic compositions ($\delta^{13}C$, $\delta^{18}O$ and Δ_{47}) of inter-skeletal elements of all echinoids are shown in Table 2.

3.1. Variation in $\delta^{13}C$, $\delta^{18}O$ in echinoid calcite

The $\delta^{18}O_{PDB}$ of distinct skeletal elements in each specimen vary (Fig. 2). One-way ANOVA tests show that differences in the $\delta^{18}O_{PDB}$ of inter-skeletal elements in echinoid orders *Diadematoida, Camarodonta and Strongylocentrotus* are statistically significant at the 95% confidence level (Table 3).

Individuals from echinoid orders *Camarodonta Strongylocentrotus* and *Clypeasteroida* exhibit linearly correlated inter skeletal $\delta^{18}O$ and $\delta^{13}C$ (Fig. 2). These groups also show an overall trend of linearly correlated $\delta^{18}O$ and $\delta^{13}C$ between different individuals ($R^2 = 0.785$, $P < 0.001$). Urchin orders *Temnopleuroida* and *Diadematoida,* collected in the Indonesian region at similar growth temperatures, show only small inter-skeletal variations in $\delta^{18}O$ (0.19‰ and 0.37‰ respectively), which are poorly correlated with differences in $\delta^{13}C$.

Inter-skeletal variation in $\delta^{13}C$ is greater than that for $\delta^{18}O$, individual skeletal elements exhibiting distinct $\delta^{13}C$ signatures (Fig. 2). In measured specimen of the order *Temnopleuroida* calcite sampled from spines has the lowest $\delta^{13}C$ of 0.41‰ while test calcite has a $\delta^{13}C$ of 1.35‰. Conversely in the measured specimen of the order *Camarodonta,* calcite with the highest $\delta^{13}C$ is found in the spines (0.81‰) while test and lantern calcite is much lighter in $\delta^{13}C$ (−0.93 to-2.22‰).

The natural logarithm of the oxygen isotope fractionation factor ($\ln1000\alpha_{\text{calcite-H20}}$) between echinoid calcite and seawater is positively correlated ($R^2 = 0.857$, $P < 0.001$), with a least-squared regression best fit equation of $\ln1000\alpha_{\text{calcite-H20}} = 14.70 \times (1000/T) - 20.13$, where 'T'

Table 2
Sample stable and clumped isotope composition.

Sample name	Order	Genus	n	$\delta^{18}O$ VPDB (‰)	S.E	$\delta^{13}C$ VPDB (‰)	S.E	Δ_{47}CDES (‰)	S.E
GA1	*Temnopleuroida*	*Tripneustes*	3	−1.59	0.04	1.16	0.02	0.710	0.006
GA2	*Temnopleuroida*	*Tripneustes*	3	−1.39	0.05	1.20	0.02	0.703	0.005
GLT	*Temnopleuroida*	*Tripneustes*	5	−1.69	0.07	0.67	0.02	0.713	0.011
GS	*Diadematoida*	*Diadema sp.*	3	−1.64	0.18	0.28	0.01	0.696	0.012
GT	*Diadematoida*	*Diadema sp.*	3	−1.32	0.17	1.25	0.06	0.710	0.012
BS	*Temnopleuroida*	*Tripneustes*	3	−1.39	0.06	0.01	0.06	0.713	0.005
BT	*Temnopleuroida*	*Tripneustes*	3	−1.75	0.10	−2.03	0.02	0.727	0.004
MA1	*Clypeasteroida*	*Dendraster*	3	1.41	0.09	−0.19	0.05	0.771	0.005
MA2	*Clypeasteroida*	*Dendraster*	3	1.49	0.10	−0.03	0.02	0.760	0.004
MB	*Clypeasteroida*	*Dendraster*	3	1.29	0.14	−0.16	0.01	0.743	0.005
ML	*Clypeasteroida*	*Dendraster*	3	1.12	0.15	−1.35	0.01	0.756	0.010
MP	*Clypeasteroida*	*Dendraster*	3	1.18	0.03	−0.69	0.05	0.763	0.012
MS	*Clypeasteroida*	*Dendraster*	3	1.03	0.08	−0.55	0.01	0.746	0.006
YA1	*Camarodonta*	*Paracentrotus*	3	0.86	0.13	−1.22	0.01	0.711	0.012
YA2	*Camarodonta*	*Paracentrotus*	4	0.69	0.07	−1.48	0.05	0.697	0.015
YLP	*Camarodonta*	*Paracentrotus*	3	1.33	0.05	−1.51	0.08	0.732	0.015
YLR	*Camarodonta*	*Paracentrotus*	3	1.00	0.05	−2.22	0.01	0.726	0.006
YLT	*Camarodonta*	*Paracentrotus*	3	0.85	0.12	−0.93	0.03	0.721	0.011
YS	*Camarodonta*	*Paracentrotus*	3	1.79	0.21	0.81	0.03	0.726	0.010
YT	*Camarodonta*	*Paracentrotus*	3	0.60	0.11	−1.64	0.02	0.735	0.005
SDA1	*Strongylocentrotus*	*Droebachiensis*	3	−0.30	0.05	−3.23	0.02	0.784	0.007
SDS	*Strongylocentrotus*	*Droebachiensis*	3	0.07	0.09	−1.32	0.01	0.755	0.002
SDA2	*Strongylocentrotus*	*Droebachiensis*	3	−0.24	0.02	−3.02	0.04	0.782	0.007
SDLT	*Strongylocentrotus*	*Droebachiensis*	3	0.03	0.10	−2.40	0.02	0.767	0.009
SDT	*Strongylocentrotus*	*Droebachiensis*	4	−0.51	0.11	−3.46	0.03	0.766	0.009

n is number of replicates.

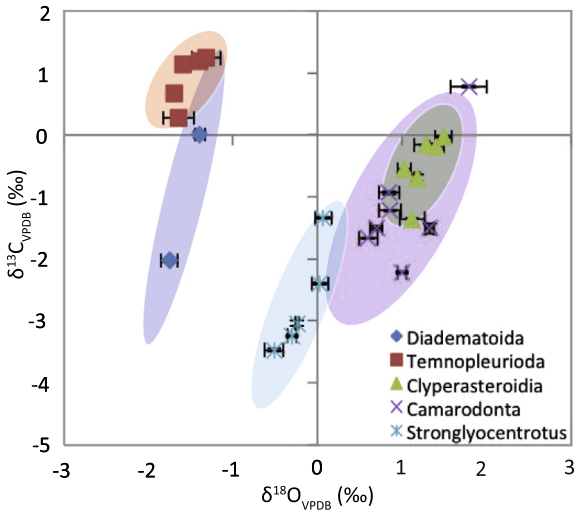

Fig. 2. Correlation between stable $\delta^{18}O$ and $\delta^{13}C$ in echinoid calcite. 90% confidence ellipses for each echinoid order are shown as shaded areas.

is temperature in K. Although oxygen isotope fractionation is correlated with temperature, $\delta^{18}O$ values of echinoid calcite are offset from temperature dependent equilibrium as established by inorganic precipitation experiments (Mavromatis et al., 2012)(Fig. 3). Four of five echinoid groups measured exhibit positive offsets in $\delta^{18}O$ in comparison with inorganic $\delta^{18}O$ calibration. The value of the offset varies between 0.65–1.25‰ in measured specimens of orders *Temnopleuroida* and *Diadematoida* to >3.7‰ in *Clypeasteroida.* The measured specimen of order *Strongylocentrotus* however exhibits a negative offset in $\delta^{18}O$ from the inorganic calibration of up to 1.34‰. As importantly, the slope of the $\ln1000\alpha_{\text{calcite-H20}}$ in echinoids differs from that of inorganic precipitation experiments (Mavromatis et al., 2012) (Fig. 3).

3.2. Inter-skeletal Δ_{47}

Individual Δ_{47} measurements of inter-skeletal elements lie within 95% confidence intervals for all echinoid species, most falling within 1σ (on average 0.0147‰, Fig. 4). One-way ANOVA tests show there is no statistically significant difference in Δ_{47} values of echinoid inter-skeletal elements at the 95% confidence level (Table 3). This is however associated with a low power value indicating low likelihood of rejecting the null hypothesis as a result of sample size. There is correspondingly no correlation between inter-skeletal $\delta^{18}O$ and Δ_{47} (Fig. 4) or $\delta^{13}C$ and Δ_{47}.

3.3. Echinoid Δ_{47}–temperature relationship

Mean Δ_{47} values of 24 inter-skeletal measurements of 5 echinoid groups are plotted versus mean annual growth temperatures (Fig. 5). A linear least squares regression of this data yields the following relationship:

$$\Delta_{47} = 0.03922 \times \frac{10^6}{T^2} + 0.2365 \quad (2)$$

($R^2 = 0.62$, $P < 0.001$) where T is temperature in K.

Table 3
Summary of ANOVA statistics for the effect of inter-skeletal element on $\delta^{18}O$ and Δ_{47} for echinoid groups measured.

ANOVA				
	DF (Groups)	DF (Error)	F-value	p-Value
Inter-skeletal Element vs. $\delta^{18}O$				
Diadema sp.	1	4	9.2783	0.0382
Tripnesutes	4	12	2.303	0.1182
Dendraster	5	12	2.6687	0.0759
Paracentrotus	6	15	12.8547	<0.001
Droebachiensis	4	11	7.6471	0.0034
Inter-skeletal Element vs. Δ_{47}				
Diadema sp.	1	4	5.0797	0.0873
Tripneustes	4	12	0.4471	0.7727
Dendraster	5	12	2.1503	0.1287
Paracentrotus	6	15	1.4311	0.2669
Droebachiensis	4	11	2.3054	0.1232

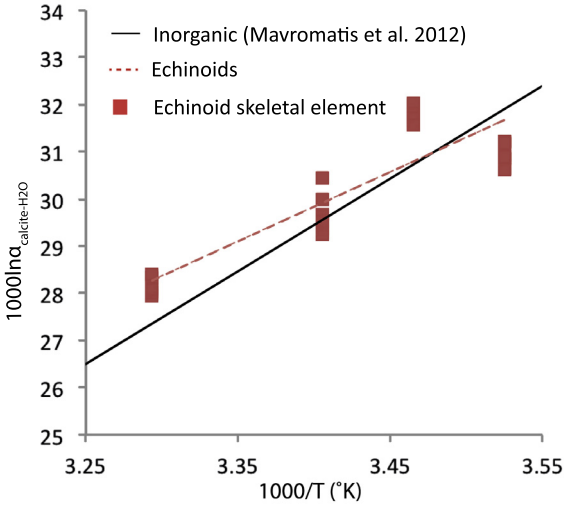

Fig. 3. Comparison of temperature dependant fractionation between calcite and water in echinoids and inorganic precipitation experiments of Mavromatis et al. (2012).

4. DISCUSSION

4.1. Echinoid Δ_{47} vs. combined inorganic calibrations

We compare the echinoid T-Δ_{47} with expected values based on the inorganic Δ_{47}-temperature calibration experiments. We chose to compare the calibrations of Kluge et al. (2015) and Kelson et al. (2017) with our echinoid dataset. These inorganic calibrations have been selected as they encompass multiple precipitation methods, cover a wide temperature range and incorporate a high density of measurements in the low temperature range (Fig. 6).

In order to allow direct comparison with other calibrations and with our own study, the Kluge et al. (2015) dataset has been re-processed using the Brand et al. (2010). ^{17}O correction parameters, and presented in the $\Delta_{47}CDES_{25C}$ reference frame using the acid fractionation factor of Defliese et al. (2015) (Annex 2). This yields the following equation:

$$\Delta_{47} = 0.03998 \times \frac{10^6}{T^2} + 0.2423 \quad (3)$$

where T is temperature in K. The Kluge et al. (2015) calibration re-proccessed using the parameters of Brand et al. (2010) is particularly useful as it was generated at Imperial College London following almost identical CO_2 purification and IRMS analyses as our echinoids measured.

An ANCOVA test conducted indicates there is significant difference between the inorganic calibrations of Kluge et al. (2015) and Kelson et al. (2017) ($F(1,81) = 2.4510$, $P = 0.1214$) correcting for temperature. Kluge et al., 2015 and Kelson et al., 2017 have no statistical difference in slope ($F(1,81) = 1.2953$, $P = 0.2585$) A student's t-test of difference in regression by least squares means between ($\alpha = 0.05$, $t = 1.98969$) verifies that there is no significant difference in intercept between the two calibrations (Table 4). Kluge et al. (2015) and Kelson et al. (2017) are thus combined to form a general inorganic calibration with equation

$$\Delta_{47} = 0.04028 \pm 0.00076 \times \frac{10^6}{T^2} + 0.23776 \pm 0.00759 \quad (4)$$

where T is temperature in K.

There is a positive offset from expected Δ_{47} values, based on our combined inorganic Δ_{47}-temperature calibration, in just over 90% of measurements of echinoid calcite. An ANCOVA test conducted indicates there is a significant difference between echinoid Δ_{47} and expected Δ_{47} based on inorganic precipitation ($F(1,108) = 15.39$, $P = 0.002$) correcting for temperature. There is however no difference in slope between the inorganic and echinoid calibrations ($F(1,108) = 0.0456$, $P = 0.8314$). We see an offset in the least squared mean value of the echinoid Δ_{47}-temperature relationship of 0.015% to higher Δ_{47} in comparison with our new combined inorganic calibration (Fig. 6).

Inter-skeletal Δ_{47} values of echinoid species based range up to 0.035‰ higher than expected based on inorganic calibration (Fig. 6). We see a much larger range in Δ_{47}-observed-expected in the measured specimen of order *Camarodonta* than in specimens of other orders. In addition converse to all other echinoid inter-skeletal measurements

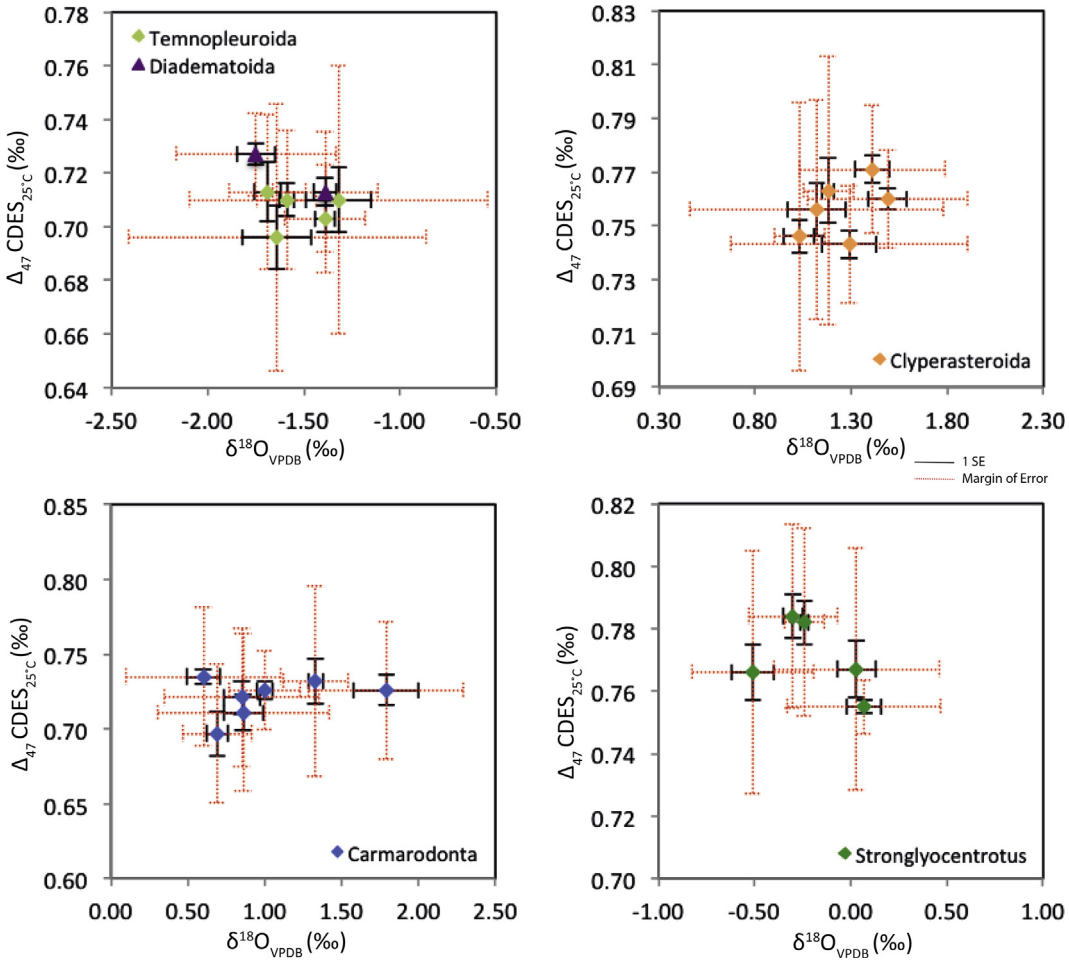

Fig. 4. Correlation between echinoid $\delta^{18}O$ and Δ_{47} for different echinoid groups. Black error bars indicate 1 SE red error bars reflect margin of error at the 95% CI. Note that Δ_{47} CDES is presented at an acid digestion temperature of 25 °C by adding a correction factor of 0.082‰ (Defliese et al., 2015). (For interpretation of the references to colour in this figure legend, the reader is referred to the web version of this article.)

Table 4
Summary of ANCOVA and sutdent t-test statistics for variation in $\delta^{18}O$ and Δ_{47} for all echinoid groups measured.

	Ancova				Student *t*-test			
	DF (Groups)	DF (Error)	F-value	p-Value	α	t	Effect size (d)	Power
Effect of inorganic calibration, Kluge et al. (2015) vs Kelson et al. (2017)	1	81	2.451	0.1214	0.05	1.98969	0.020200463	0.0505
Vital effects in Δ47-T calibration, echinoids v.s inorganic calibration	1	108	15.39	0.002	0.05	1.9826	0.4251	0.3135

in all groups ambulacral and inter-ambulacral calcite of the measured specimen of the order *Camarodonta* are lower Δ_{47} in comparison with expected values. We propose that this is an artifact of our method of growth temperature estimation which is based on an average of seasonal temperatures. There is much greater seasonal SST variation in the Mediterranean Sea than at other collection localities. This may explain the greater variation in Δ_{47} of inter-skeletal calcite in the measured specimen of order *Camarodonta* assuming different inter-skeletal growth periods. Skeletal growth in warm summer periods may also explain apparent depletion Δ_{47} in comparison with expected values in the measured specimen of order *Camarodonta*.

4.2. Echinoid Δ_{47} vs. other biogenic calibration data sets

We compare our echinoid Δ_{47} dataset with biogenic datasets presented in the absolute reference frame (Fig. 7). In order to allow direct comparison between data sets we re-process our echinoid dataset using the Santrock et al. (1985) ^{17}O correction parameters and compare with the Kelson et al. (2017) and inorganic calibration processed

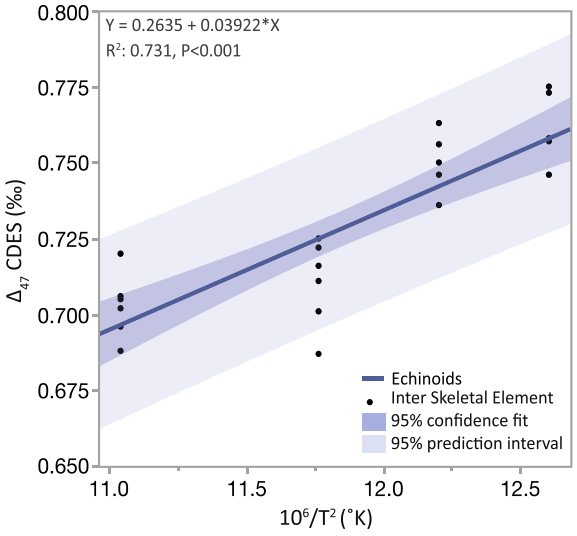

Fig. 5. Correlation between temperature and Δ_{47} in echinoids. Black data circles represent clumped isotope measurements of inter-skeletal elements of each echinoid order comprising 3–4 replicates.

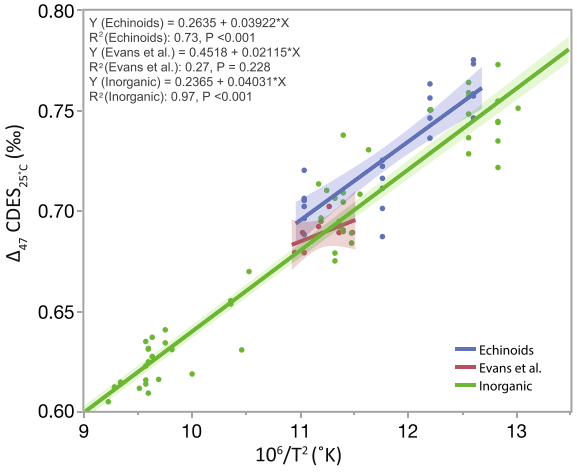

Fig. 6. Correlation between temperature and Δ_{47} in echinoids, the combined inorganic calibration of Kluge et al. (2015) and Kelson et al. (2017) and Evans et al. (2018). Δ_{47} CDES is presented at 25 °C acidification temperature by adding the acid fractionation factor 0.082 (Defliese et al., 2015). Note the negligible overlap in confidence fits between the echinoid inorganic calibrations and 0.015% positive offset of the echinoid calibration.

using the Santrock parameters. All values are corrected to acid digestion at 25 °C using the AFF 0.082‰ (Defliese et al., 2015). The positive offset in Δ_{47} in echinoids is in the in the same direction but 0.025‰ lower than the positive offsets observed in aragonitic scleractinian corals (Kimball et al., 2015) shallow water corals (Saenger et al., 2012) and brachiopods (Came et al., 2014) at 25 °C. Cephalopods (Dennis et al., 2013) are offset to lower than expected values of Δ_{47} by 0.02‰ and , an offset in the opposite direction but of similar magnitude to that observed in the echinoids (Table 5).

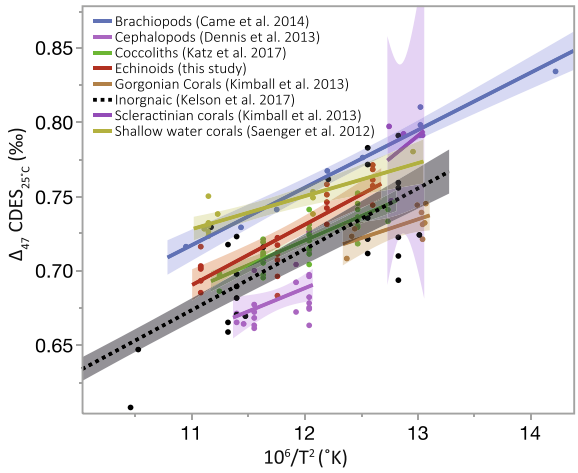

Fig. 7. Correlation between temperature and Δ_{47} in echinoids (red line) compared to other biomineralizing groups with Δ_{47} CDES in the absolute reference scale of Dennis et al. (2011). All data are presented in the 25 °C reference frame adjusting the acid fractionation factor to a common 0.082‰(Defliese et al., 2015) using Santrock et al., 1985 17O correction parameters. Shaded errors reflect 95% confidence limits on regression. (For interpretation of the references to colour in this figure legend, the reader is referred to the web version of this article.)

4.3. Sources of positive offset in Δ_{47}

4.3.1. Potential effects of sample preparation, processing and IRMS analysis

Measurement of echinoid Δ_{47} made at Imperial College following similar laboratory procedure as Kluge et al. (2015) enables us to discount difference in sample processing and IRMS analysis as a potential cause in deviation of echinoid Δ47 from inorganic values. Most analysis of Kluge et al. (2015) and all analysis of Kelson et al. (2017) were acidified at 90 °C, the acidification temperature used in this study. This removes the complication of accurately determining the difference in acid fractionation factor between 90 and 25 °C in comparing inorganic and biogenic calibrations. Our study also uses the same acid digestion technique, purification by a static PPQ trap without helium flow at −35 °C, ^{17}O correction parameters in raw data processing and carbonate standards for translation into the absolute reference frame as the inorganic calibration of Kluge et al. (2015). This enables us to make a more meaningful comparison of inorganic and biogenic datasets.

There is no systematic offset to higher Δ_{47} in ambulacral and interambulacral elements drilled with a low speed dental drill in comparison with bulk test samples powdered with a pestle and mortar (Table 2). It may therefore be concluded that sample preparation by low speed drilling does not result in resetting of calcite Δ_{47}.

4.3.2. Effect of mineralogy

Echinoderm skeletal elements are composed of Mg-enriched calcite, content ranging between 3.0–18.5 mol% magnesium (Clarke and Wheeler, 1917; Chave, 1954; McClintock et al., 2011) with up to 43.5 mol%

Table 5
Overview of differences between biogenic Δ_{47}-T calibration datasets processed using the Santrock et al. (1985) parameters.

Calibration	*Equation of the Calibration Line*				
	Gradient (a)	Intercept (b)	Δ_{47} offset (‰)[a]	Temperature offset (°C)[b]	Higher (H) or lower (L) apparent temperature
Brachiopods (Came et al., 2014)	0.03873	0.2908	0.041	6.73	L
Cephalopods (Dennis et al., 2013)	0.03123	0.3131	−0.027	−4.64	H
Coccoliths (Katz et al., 2017)	0.03307	0.3232	0.006	0.95	L
Echinoids (this study)		0.0407	0.2422	0.017	2.76
Gorgonian Corals (Kimball et al., 2013)	0.02526	0.4059	−0.006	−0.97	H
Inorgnaic (Kelson et al., 2017)	0.04097	0.2224	0.000	0.00	n/a
Scleractinian corals (Kimball et al., 2013)	0.06158	−0.0102	0.016	2.61	L
Shallow water corals (Saenger et al., 2012)	0.02226	0.4827	0.035	5.72	L

Calibration equations in the linear form a = mx + b.
[a,b] offset calculated at 15 °C.

"proto-dolomite" measured in axial zones of echinoid teeth (Schroeder et al., 1969).

Equilibrium constants for the equilibrium exchange reaction $M^{13}C^{16}O_3 + M^{12}C^{18}O^{16}O_2 \rightleftharpoons M^{13}C^{18}O^{16}O_2 + M^{12}C^{16}O_3$, where M is Ca or Mg in calcite, dolomite and aragonite have been calculated to be relatively constant with crystal chemistry. The equilibrium constant for the above reaction is 0.004‰ lower in dolomite than in calcite (Schauble et al., 2006). This deviation equates to differences in mineral Δ_{47} one order of magnitude smaller and in the opposite direction to observed Δ_{47} excesses in echinoid high-Mg calcite. Mineral specific differences in isotopic fraction during phosphoric digestion have also been predicted (Guo et al., 2009; Tripati et al., 2015). At 25 °C theoretically predicted $\Delta_{47calcite} - \Delta_{47dolomite} \approx 0.022‰$, a deviation of the same order of magnitude but again in the opposite direction to differences observed between echinoid Δ_{47} and inorganically precipitated calcite (Guo et al., 2009; Tripati et al., 2015) (Fig. 9). We therefore conclude that the discrepancy in the biogenic calibration of the echinoids does not relate to mineralization as high-Mg calcite. This is further supported by the lack of offset between benthic forams measured by Evans et al. (2018), also composed of high Mg-calcite, and the combined inorganic calibration of Kluge et al. (2015) and Kelson et al. (2017) (Fig. 6).

4.3.3. Effects of CO_2 source and diffusion into calcifying sites

Echinoid biomineralization occurs in a vacuole enclosed in a syncytial pseudopodium composed of skeletal cells (sclerocytes), a membrane envelope produced by many cells. The mineralization site is thus isolated from the environment, sclerocytes controlling of ion balance and liquid volume (Wilt, 2002; Politi et al., 2004). Skeletal tissue is separated from the external medium by an epidermis and the inner medium (body cavity) by a mesothelium.

The process of diffusion of CO_2 dissolved in seawater across the calioblastic membrane into the calcifying fluid has been suggested as a potential mechanism causing kinetic fractionations in Δ_{47} in corals (Thiagarajan et al., 2011; Saenger et al., 2012). Thiagarajan et al. (2011) calculated resultant fractionations of liquid phase diffusion amounting to 1.6‰ in $\delta^{18}O$ and +0.036‰ for Δ_{47}

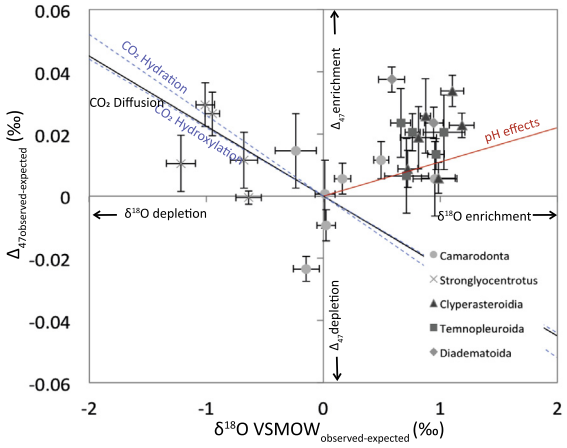

Fig. 8. Correlation between fractionation in $\delta^{18}O$ and Δ_{47} in echinoids. Vector trajectories for effects of different processes on stable isotope signatures such as pH effects (Tripati et al., 2015), CO_2 diffusion (Thiagarajan et al., 2011), CO_2 hydration and hydroxylation reactions (Guo et al., 2008). Y-error bars represent propagated error on calculated expected Δ_{47} based on calibration error, error in growth temperature and standard error on Δ_{47} observed. X-error bars represent propagated error on expected $\delta^{18}O$ based on error in $\delta^{18}O_{sw}$ at growth location, error on $\delta^{18}O$ calibration and observed $\delta^{18}O$ measured at Imperial College London.

(Fig. 8). The positive offset in Δ_{47} is similar to our observations in the echinoids, however we observe a correlated enrichment in $\delta^{18}O$ in contrast to depletion (Figs. 3 and 8). Stumpp et al. (2012) demonstrate that the outer epidermis in echinoid larvae is semi-porous, allowing seawater DIC to pass directly and to flood the extracellular compartment surrounding calcifying scelerocytes. This may contribute to the lack of a diffusive signature in echinoid $\delta^{18}O$ and Δ_{47}.

Stable isotopic data from Courtney and Ries (2015) illustrates that increasing pCO_2 affects the correlation between $\delta^{13}C$ and $\delta^{18}O$ in echinoid calcite. At higher pCO_2 concentrations we observed a steeper correlation in

the $\delta^{13}C$ and $\delta^{18}O$ relationship. Echinoids lack a structurally complex respiratory system, where CO_2 transport is facilitated by perivisceral coelomic fluids, the fluids composing the main body cavity of the echinoid (Weber, 1968). We propose that more positive $\delta^{13}C$ at increased pCO_2 may occur as a result of increased diffusion of environmental CO_2 into calcifying sites mixing linearly with lighter respiratory CO_2 produced at a constant rate independent of cellular pCO_2.

4.3.4. Kinetic effects during hydration/hydroxylation

Intra-specimen correlation between $\delta^{18}O$ and $\delta^{13}C$ reported here (Fig. 2) has been previously documented. Linearly correlated variations in skeletal $\delta^{18}O$ and $\delta^{13}C$ in cidaroid urchins are purported to relate to kinetic effects during the hydration and hydroxylation of CO_2 (McConnaughey, 1989a; McConnaughey, 1989b) calculated to be the rate-limiting step in inorganic carbon speciation (Johnson, 1982).

If kinetic effects during hydroxylation and hydration of CO_2 purported to offset biogenic calcite $\delta^{18}O$ and $\delta^{13}C$ from equilibrium precipitation have a measurable effect on echinoid Δ_{47}, we might expect to see correlated relationships between these variables and echinoid Δ_{47} both inter-skeletally and between species. Hydration affects the isotopic composition of CO_2 diffusing into the calcifying site, thus the overall composition of the DIC. Likewise dehydration followed by degassing also effects the overall composition of the DIC. The hydration/dehydration of CO_2 has been demonstrated to occur at the same rate for Δ_{47} as $\delta^{18}O$ suggesting disequilibrium in one system will also manifest in the other (Affek, 2013) and is postulated to be a contributory factor in measured positive Δ_{47} offsets in surface corals (Saenger et al., 2012). Kinetic effects during hydration/dehydration result in enrichment in Δ_{47} and associated depletion $\delta^{18}O$. This is converse to the enrichment in both $\delta^{18}O$ and Δ_{47} observed in most echinoid data (Fig. 8). Inter-skeletal calcite from the cold-water echinoid *Stronglyocentrotus* grown at 8.5 °C does however show more depleted $\delta^{18}O$ and enriched Δ_{47} compared to inorganic calcite equivalent, implying the potential action of kinetic effects during precipitation particularly in $\delta^{18}O$. The manifestation of kinetic effects is dependent on the ratio of the rate of precipitation to the rate of isotopic equilibration of the DIC pool. The timescale of equilibration of DIC in solution is longer at lower temperature (Zeebe and Wolf-Gladrow, 2001) thus it is a reasonable assumption that kinetic effects may play a role in observed "vital effects" in echinoids growing fast at lower water temperatures.

4.3.5. pH effects

The fluid composition of isolated environments such as calcification sites in echinoids has the potential to yield significant deviation in fluid composition from seawater values, including variable pH and ion concentration. This allows for significant variation in the DIC pool from with the mineral precipitates compared to external seawater.

The calcifying fluid DIC solution consists of carbonic acid (H_2CO_3) dissolved carbon dioxide ($CO_{2(aq)}$), bicarbonate (HCO_3^-) and carbonate (CO_3^{2-}) ions. Theoretical modelling by Hill et al. (2014) indicates each DIC species has a distinct equilibrium clumped isotope signature, Δ_{47} (H_2CO_3) > Δ_{47} (HCO_3^-) > Δ_{47} (equilibrium calcite) > Δ_{47} (CO_3^{2-}), thus speciation within the parent DIC pool has the potential to affect clumped isotope composition of precipitating carbonate minerals (Hill et al., 2014). The difference between $\Delta_{47}(HCO_3^-)$ and Δ_{47} (CO_3^{2-}) at 25 °C is predicted to be 0.018‰ (Guo et al., 2008) to >0.033‰ (Hill et al., 2014). The effect of varying pH alters the partitioning of DIC species according to equilibrium constants pK_1 and pK_2. A decrease in pH would shift equilibrium to the left favouring the formation of H_2CO_3 over HCO_3^- (Eq. (5)) and HCO_3^- over CO_3^{2-} (Eq. (6)) (Millero et al., 2006; Hill et al., 2014). Calculations of the Δ_{63}, defined as the per mil deviation in the abundance of all CO_3^{2-} isotopologues from the abundance predicted by random mixing, for the composite DIC pool, indicates increased Δ_{63} with decreases in pH. This effect is amplified at increased salinities (S = 35,50) (Hill et al., 2014).

$$CO_2 + H_2O \rightleftharpoons\rightleftharpoons H^+ + HCO_3^- \quad (5)$$

$$HCO_3^- \rightleftharpoons\rightleftharpoons H^+ + CO_3^{2-} \quad (6)$$

It has been hypothesized that pH effects could explain observed variations in Δ_{47} and $\delta^{18}O$ in deep-sea corals (Thiagarajan et al., 2011). Coral calcification is associated with an increase of the pH of the calcifying fluid (pH_{cf}) from seawater pH ($pH_{sw} \sim 8.1$) (Marion et al., 2011). The pH_{cf} in corals has been investigated using the boron isotopic pH proxy and has been found to range between 8.3 and 8.5 (McCulloch et al., 2012; Holcomb et al., 2014; Sutton et al., 2017) while microelectrode measurements of scleractinian coral species indicate they elevate pH_{cf} by 1–2 units relative to pH_{sw} (Al-Horani et al., 2003; Ries, 2011). The effects of pH_{cf} in corals thus tend to a general decreases in Δ_{63} (Fig. 10) (Hill et al., 2014). Using the boron isotope proxy, tropical echinoids pH_{cf} has been shown to be only 0.1 units greater than pH_{sw}, whereas temperate echinoids pH_{cf} tends to be 8.0, lower than pH_{sw} (Sutton et al., 2017). Assuming the Δ_{63} signature of the DIC is directly inherited during mineral precipitation i.e. precipitation occurs fast enough that calcite crystals do have time to come to internal bulk equilibrium, a decrease in pH_{cf} in echinoids is in agreement with higher than expected Δ_{47} of echinoid calcite (Hill et al., 2014) (Fig. 10). It must be noted however that based on the model of Hill et al. (2014) the offset in Δ_{47} from equilibrium at pH values ~8.6 is at its maximum 0.009‰, almost 3 times lower than Δ_{47} enrichment observed in the echinoids.

Experimental results however indicate a difference in Δ_{47} (thus Δ_{63}) between CO_3^2 and HCO_3^- of 0.063 ± 0.006‰ (Tripati et al., 2015), twice that of theoretical predictions, suggesting greater magnitude effects of variations in pH_{cf} on Δ_{47}. The observed slope of Δ_{47} observed-expected against $\delta^{18}O$ observed-expected, excluding anomalous *Stronglyocentrotus* samples, is remarkably similar to the

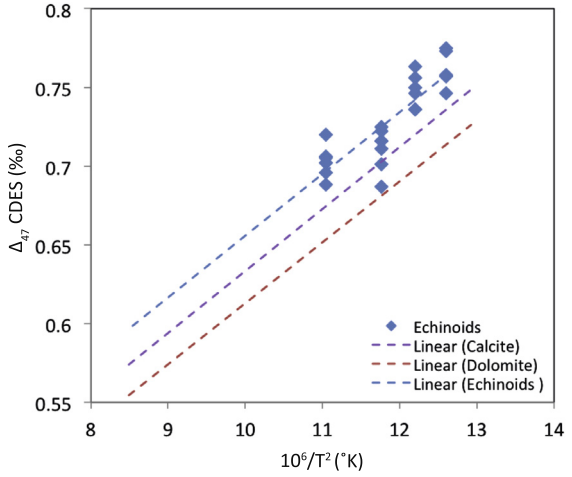

Fig. 9. Echinoid Δ_{47}-temperature relationship in comparison with theoretical calcite and dolomite (Guo et al., 2009).

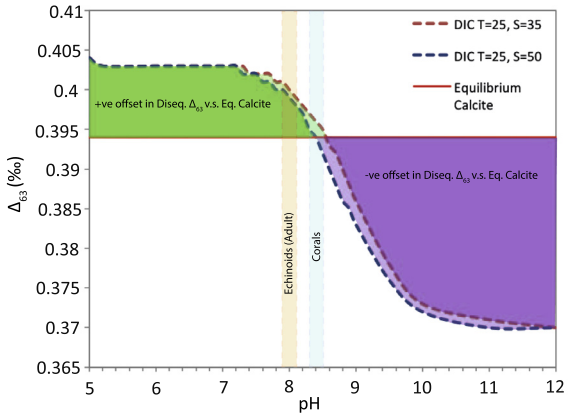

Fig. 10. pH dependence of Δ_{63} of DIC (Hill et al., 2014). Shaded boxes show pH_{cf} echinoids (Sutton et al., 2017) and corals (Al-Horani et al., 2003; Ries, 2011).

observed slope of regression (0.011 ± 0.001) of synthetic witherite precipitation at variable pH (Fig. 10) (Tripati et al., 2015).

It may therefore be concluded that pH effects relating to direct inheritance of the Δ_{63} signature from the DIC may contribute to but may not be the sole cause of enrichments in echinoid Δ_{47} from expected values. The potential for observable pH effects is greater at increased salinities (Tripati et al., 2015, Hill et al., 2014).

4.3.6. Precipitation/calcification rate

Echinoid $\Delta^{18}O$ ($\Delta^{18}O = \delta^{18}O_e - {}^{18}O_{DIC}$) is weakly negatively correlated with calcification rate (Courtney and Ries, 2015). Likewise in inorganic precipitation experiments, oxygen isotope fractionation has been demonstrated to depend on precipitation rate (R) ($1000 \ln \alpha_{calcite-water} = 1.094 \log R + 30.87$ (Dietzel et al., 2009). As echinoids measured as part of this study were mostly collected live from the benthos, measurement of precipitation rate and comparison with Δ_{47} offset has not been possible. Previous studies however indicate that echinoids are capable of rapid calcite precipitation, the inner stereom of snapped spines calcifying at a longitudinal rate of 125 μm/day (Gorzelak et al., 2011). Courtney and Ries (2015) give an approximation of growth rate of the bulk shell reporting up to a 0.504% d^{-1} change in buoyant weight over a 60 day period in adult *Echinometra viridis* while juvenile *Tripneustes gratilla* calcify at up to 2.75% d^{-1}. If calcite crystals precipitate slowly enough to reach internal bulk equilibrium, their Δ_{47} will remain independent of the Δ_{63} of the DIC and by extension of the pH of the parent solution (Tripati et al., 2015). This may explain why correlated $\delta^{18}O$-Δ_{47} effects relating to pH of the calcifying fluid appear to manifest in rapidly calcifying echinoids but not in other groups.

Crystal growth models such as the growth entrapment model (Watson and Liang, 1995; Watson, 2004; Gabitov, 2013) and surface kinetic models (DePaolo, 2011) link net precipitation rate to potential disequilibrium in isotopic signatures when growth rates are high. Ion-by-ion growth models (Watkins and Hunt, 2015), assuming attachment and detachment rate coefficients for HCO_3^- and CO_3^{2-} isotopologues, are useful in explaining disequilibrium signatures in biological carbonates considering predicted differences in bond ordering between the two ions. Experimental results based on inorganic precipitation under varying conditions however do not capture differences in Δ_{47} as a result of growth effects eg precipitation rate (Tang et al., 2014) whilst others indicate temperature dependent Δ_{47}-$\delta^{18}O$ co-variance indicating additional fractionation in fast growing minerals that effects in $\delta^{18}O$ but not Δ_{47} (Affek and Zaarur, 2014).

4.3.7. Other potential effects

A notable feature of echinoid biomineralization is crystal formation via an initial amorphous calcium carbonate (ACC) phase on an organic matrix. ACC is formed as a transient precursor phase both in echinoderms (Beniash et al., 1997; Politi et al., 2004) and some bivalve molluscs (Weiss et al., 2002). The appearance of this biomineralization mechanism on two different branches of the phylogenetic tree indicates that, although difficult to diagnose, it may be widespread amongst invertebrates (Raz et al., 2003). The formation of ACC and hindrance of conversion to more stable crystalline phases requires unique conditions such as the creation of a microenvironment disfavoring organization of nuclei (Addadi et al., 2003) or the introduction of additives for example ions or organic macromolecules add that interfere with crystal growth (Raz et al., 2003). Despite our lack of understanding of exactly how ACC forms (Addadi et al., 2003) it is conceivable that either of these mechanisms may act to promote a unique Δ_{47} signature independent of environmental conditions.

The mechanism by which ACC is converted into calcite remains uncertain (Addadi et al., 2003). Further knowledge of how this occurs is important as it may determine whether the potentially unique Δ_{47} composition in ACC is inherited. If ACC is converted to calcite by dissolution and re-precipitation in interaction with water in an open system then Δ_{47} composition of ACC will be lost. If however this conversion occurs under closed conditions, i.e. within a

closed cellular compartment, or without breaking of C—O bonds, preservation of a unique non-environmentally representative Δ_{47} signal may still occur. In urchin larval spicules the growing spicule is initially composed of ACC prior to the propagation of a single crystal through the ACC phase without evidence of an identifiable crystallisation front (Beniash et al., 1997). This occurs within the isolated environment of the confining vesicle so the ACC is not in contact with the surrounding aqueous solution. Likewise $CaCO_3$ is delivered to the spicule forming compartment as pre-formed ACC, also confined to vesicles thus preventing interaction with the surrounding environment (Beniash et al., 1997). Stabilisation to calcite is thought to occur by breakdown, conversion or rearrangement of macromolecules (Raz et al., 2003). The occurrence of this process in isolation favours preservation of the initial Δ_{47} signal of ACC.

Matrix macromolecules in the presence of magnesium ions have been demonstrated to be responsible for the formation and stabilization of ACC in sea urchin larval spicules (Raz et al., 2003). An experimental study by Wang et al. (2009) indicates that Mg content in biogenic ACC is regulated by macromolecules including carboxylated (acidic) proteins. Mg/Ca ratios appear to be controlled by a predictable dependence on binding properties of organic molecules related to electrostatic topology. It is reasonable therefore to assume that electrostatic topology of the organic mineralization matrix in groups such as echinoids could have an influence in the adsorption of CO_3^{2-} and/or HCO_3^- isotopologues into the calcite surface thus impacting Δ_{47}. We however do not observe any relationship between offsets in Δ_{47} and Mg/Ca ratio in echinoid inter-skeletal elements as reported by Weber (1969). Kimball et al. (2015) measured the clumped isotope composition of Gorgonian corals that, like the echinoids, form high-Mg calcite on an organic matrix. The gorgonians display an offset in Δ_{47} opposite in polarity to that observed in the echinoids (Kimball et al., 2015) thus it is difficult to reconcile the two with the same mechanism. It is however notable that both display discernable offsets from the inorganic Δ_{47} calibration in comparison with equilibrium precipitators such as coccoliths (Katz et al., 2017) and benthic forams (Evans et al., 2018).

4.4. Perspective for the use of echinoderm Δ_{47} in paleoclimate reconstruction

Echinoderms offer good targets for paleoclimate reconstruction as a result of their relatively high abundance and ubiquitous distribution in most marine facies (Lebrato et al., 2010) and long fossil record, dating back to the Early Cambrian (Bottjer et al., 2006). The echinoderm origin of sediment particles can be recognised by their characteristic microstructure. They are an important component of Cenozoic carbonate systems and can compose between 5 and 30% of sediment particles (Kroh and Nebelsick, 2009). Echinoids are particularly common in Oligo-Miocene carbonates, clyperasteroids forming mass occurrences in shore face sequences, which can be up to several metres in thickness (Nebelsick and Kroh, 2002).

The high-Mg calcite composition of echinoderms is thermodynamically metastable under environmental conditions, however recrystallization during early diagenesis is often inhibited by organic and inorganic linings (Berner, 1966; Weber, 1969). Cement coating plays an important role in preservation, forming so called "crystal caskets" that prevent ion exchange with echinoderm calcite and surrounding pore water (Dickson, 2001). Dickson et al. (1995, 2004) report examples dating back to the Silurian where echinoderm high Mg-calcite has been preserved enabling the application of stable isotope techniques. Furthermore diagenetic recrystallization is easier to detect in organisms composed of high-Mg calcite as this is rapidly converted to low-Mg, low-Sr calcite with no continuum in Mg/Ca-Sr/Ca space between well-preserved and poorly preserved samples. Mg/Ca and Sr/Ca ratios can thus been used to identify recrystallized samples (Evans et al., 2018).

Variability in fractionation of $\delta^{18}O$ both inter-skeletally and between individuals combined with uncertainties in the $\delta^{18}O_{sw}$ of ancient oceans however serves to complicate paleotemperature reconstruction based solely on stable oxygen isotopic composition of skeletal calcite. Previous studies indicate strong vital effects in $\delta^{18}O$ and $\delta^{13}C$ with high inter-specific, inter-specimen and inter-skeletal variation. This variation is controlled by a variety of factors, largely genetic but also including temperature, depth of growth, food supply and ambient $\delta^{13}C$- level and is thus non-predictable (Weber and Raup, 1966a; Weber and Raup, 1966b; Weber, 1968). The most significant correlation of $\delta^{18}O$ with temperature is observed in test calcite ($r^2 = -0.34$, $N = 153$) (Weber and Raup, 1966b).

The clumped isotope composition of echinoid calcite is shown to be homogenous inter-skeletally (Fig. 4). Additionally, although the clumped isotopic composition of echinoid calcite shows a positive small offset from expected values based on inorganic precipitation experiments, the positive Δ_{47} offset is consistent among echinoid groups. The offset in echinoid Δ_{47} may thus be corrected for either by deducting 0.015‰ from echinoid Δ_{47} values prior to applying our inorganic Δ_{47}-T calibration. This offset, although small, is statistically robust at 0.0146 ± 0.0042‰. The error calculated on this offset using a least squared means student t-test adds only a ±0.31 °C uncertainty on the total propagated temperature error of our inorganic calibrations (Kluge et al., 2015; Kelson et al., 2017). Moreover in contrast to echinoid $\delta^{18}O$ calibration, the offset in echinoid Δ_{47} from the inorganic calibration is constant across the range of measured temperatures (i.e. both the echinoid and inorganic calibrations have indistinguishable slopes). This predictable offset makes echinoid Δ_{47} a more reliable temperature proxy than echinoid $\delta^{18}O_{VPDB}$. Vital effects in echinoid $\delta^{18}O$ however still remain a barrier to the use of combined Δ_{47} and $\delta^{18}O_{VPDB}$ to back calculate $\delta^{18}O_{sw}$. The positive 0.015‰ offset of echinoid calcite from the organic calibration is only demonstrated here within a 8.5 °C to 28 °C range of growth temperature, and thus applications beyond this range requires extrapolation of the data or further study to validate the application of the clumped isotope proxy to echinoids growing at very low sea temperatures (1–2 °C).

5. CONCLUSIONS

This study is the first to systematically measure echinoid Δ_{47}. The inter-skeletal variation in Δ_{47} is insignificant. We find however a positive offset of 0.014‰ in Δ_{47} relative to the inorganic calibration of the clumped isotope thermometer, corresponding to approximately a 4.5 °C underestimation of precipitation temperature at 15 °C. Although small the 4.5 °C underestimate in growth temperature observed based on clumped isotopic composition is consistent across echinoid orders, both regular and irregular. The magnitude of positive Δ_{47} offset in the echinoids is approximately half that of the positive Δ_{47} offsets reported in brachiopods and shallow water corals (Saenger et al., 2012; Came et al., 2014). This offset is however statistically significant and cannot be explained by inter-laboratory differences in calibration or mineralogical differences. Four of five echinoid species measured in this study show enrichment in Δ47 of echinoid calcite associated with corresponding enrichment in $\delta^{18}O$. Neither kinetic effects during hydroxylation of CO2 nor isotopic fractionation during CO2 diffusion into calcifying sites can explain this pattern. Enrichments in Δ_{47} and $\delta^{18}O$ of the magnitude observed may however correspond to pH effects on DIC speciation in the calcifying fluid in association with rapid precipitation rate and potential effects relating to ACC precipitation on an organic matrix. Depletion in $\delta^{18}O$ and enrichment in Δ_{47} of skeletal elements of echinoid *Stronglyocentrotus* may also imply potential kinetic effects during rapid precipitation at very low growth temperatures.

Based on our results, we suggest that the echinoids may be added to a growing list of calcifying groups that show evidence of an offset in clumped isotope composition in comparison with inorganic precipitation experiments. This offset is however constant across growth temperature range of species measured and can thus easily be corrected. This suggests that Δ_{47} in echinoids may be a more reliable temperature proxy than $\delta^{18}O_{VPDB}$. The addition of a further group to the growing list of organisms showing statistically distinguishable "vital effects" in Δ_{47} is proof that these effects are more widely spread than at first conceived.

ACKNOWLEDGEMENTS

This research was funded by the Engineering and Physical Sciences Research Council (EPSRC), grant number EP/M506345/1. The authors would like to thank Steve Eddy from the Centre for Cooperative Aquaculture Research at the University of Maine for agreeing to and organizing the provision of echinoids grown by aquaculture, Simon Davies, Claire Veillard and Maria Gusarevich for help in the lab. We would also like to thank Hagit Affek and the anonymous reviewer, the suggestions of whom improved this paper resulting in its current form.

APPENDIX 1

Statistical methods

In one way-ANOVA tests we report DF(Groups), DF (Error), F-values and p-values following APA style (American Psychological Association, 1994). DF(Groups) gives the between group variation calculated as k-1, DF (Error) gives the within group variation N-k. The F-Statistic gives variation between sample means/variation within samples thus comparing the variability between groups to the variability within groups. Low F-values indicate close group means however in order to interpret F-values we present the p-value. The p-value gives the probability of obtaining a value above the F-value on the F-distribution, which follows the ratio of between group variability to within group variability assuming the null hypothesis is true. P-values of >0.05 or >0.01 enable us to reject the null hypothesis at the confidence level of 95% or 99% respectively.

When assessing suitability of one-way ANOVA in analyses we must consider the effect of sample size. The "effect size" quantifies the difference between groups emphasizing the size of the difference free of sample size effects. We can calculate the effect size between groups η^2.

$$\eta^2 = \mathrm{SS(Between\,groups)/SS(Total)} \quad (1)$$

where SS(Between groups) is the sum of squares for the effect of the independent variable and SS(Total) is the total sum of squares (Richardson, 2011).

In one-way ANOVA analyses we, on average, test 5–6 groups, each representing a skeletal element with 3–4 replicates in each group. Effect size varies from 0.2 to 0.29, a medium effect size (Cohen, 1992). Power values for ANOVA analyses in this study are <0.2 at a significance level of 0.05. Low power values indicates a high probability of type II errors manifested and less than a 0.2 chance of rejecting the null hypothesis. We however present the results of these statistical tests as a first step to more quantitative analysis of clumped datasets.

The coefficient of determination (R^2) (Eq. (2)) is used to quantify the significance of association between two continuous variables x and y such as temperature and Δ_{47}. Assessment of correlation is important in identifying covariates.

$$R^2 = \left(\frac{n(\Sigma xy) - (\Sigma x)(\Sigma y)}{\sqrt{\left[n\Sigma x^2 - (\Sigma x)^2\right]\left[n\Sigma y^2 - (\Sigma y)^2\right]}} \right)^2 \quad (2)$$

ANCOVA is a parametric test assuming independent observations and that the covariate and dependent variable are linearly related with equal slope. In the case of this work, this implies testing the difference in Δ_{47}-temperature calibrations where inorganic and biogenic calibrations form independent categorical variables, Δ_{47} is the dependent variable and temperature is the covariate. As in one way ANOVA analyses we report DF(Groups), DF(Error), F-values and p-values.

To further verify ANCOVA results we carry out student t-tests on least squared mean difference between the two groups tested. As for ANOVA can test for effect size

$$\mathrm{d} = \mathrm{m_a} - \mathrm{m_b}/\sigma \quad (3)$$

where d is effect size m_a is group a mean m_b is group b mean and σ is pooled standard deviation $\sigma = \sqrt{[(\sigma_a - \sigma_b)/2]}$.

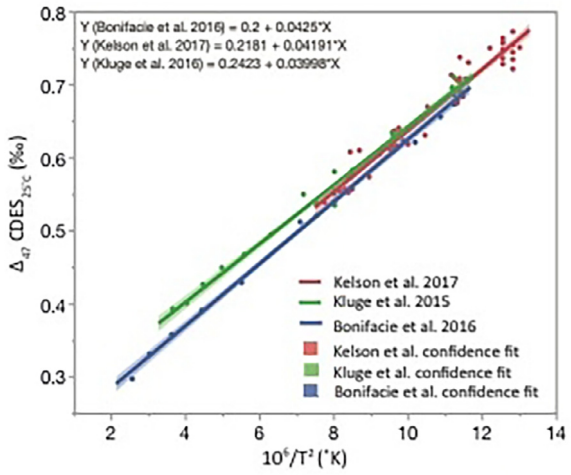

Fig. 1a. Correlation between temperature and Δ_{47} in echinoids and the inorganic precipitation experiments of Kluge et al. (2015) and Kelson et al. (2017). Δ_{47} CDES is presented at 25 °C acidification temperature by adding the acid fractionation factor 0.082 (Defliese et al., 2015) Note that while the shaded confidence fits of inorganic calibration regression lines coincide there is only some overlap between confidence fit on the echinoid calibration regression and that of the inorganic calibrations.

Creation of a re-processed inorganic Δ_{47} calibration

We choose to compare our echinoid calibration with the inorganic calibrations of Kluge et al. (2015), re-processed using the Brand et al. (2010) ^{17}O correction parameters and Kelson et al., 2017. In order to determine if combining these calibrations to form a combined low temperature inorganic calibration was a valid approach we carry out statistical tests determining there is no significant difference between the two calibrations. Fig. 1a plots both calibrations.

The T-Δ_{47} calibration of (Bonifacie et al., 2016) for dolomite is also shown (Fig. 1a) however is not incorporated into the combined inorganic calibration owing to the deviation from Kluge et al. (2015) at high temperature.

REFERENCES

Addadi L., Raz S. and Weiner S. (2003) Taking advantage of disorder: amorphous calcium carbonate and its roles in biomineralization. *Adv. Mater.* **15**, 959–970.

Affek H. P. (2013) Clumped isotopic equilibrium and the rate of isotope exchange between CO_2 and water. *Am. J. Sci.* **313**, 309–325.

Affek H. P. and Eiler J. M. (2006) Abundance of mass 47 CO_2 in urban air, car exhaust, and human breath. *Geochim. Cosmochim. Acta* **70**, 1–12.

Affek H. P. and Zaarur S. (2014) Kinetic isotope effect in CO_2 degassing: insight from clumped and oxygen isotopes in laboratory precipitation experiments. *Geochim. Cosmochim. Acta* **143**, 319–330.

Al-Horani F. A., Al-Moghrabi S. M. and de Beer D. (2003) The mechanism of calcification and its relation to photosynthesis and respiration in the scleractinian coral Galaxea fascicularis. *Mar. Biol.* **142**, 419–426.

American Psychological Association, 1994. Publication Manual of the American Psychological Association. Amer. Psychological. Assn.

Beniash E., Aizenberg J., Addadi L. and Weiner S. (1997) Amorphous calcium carbonate transforms into calcite during sea urchin larval spicule growth. *Proc. Roy. Soc. B-Biol. Sci.* **264**, 461–465.

Berner R. A. (1966) Diagenesis of carbonate sediments: interaction of magnesium in sea water with mineral grains. *Science* **153**, 188–191.

Bonifacie M., Calmels D., Eiler J. M., Horita J., Chaduteau C., Vasconcelos C., Agrinier P., Katz A., Passey B. H., Ferry J. M. and Bourrand J.-J. (2016) Calibration of the dolomite clumped isotope thermometer from 25 to 350 °C, and implications for a universal calibration for all (Ca, Mg, Fe)CO_3 carbonates. *Geochim. Cosmochim. Acta*, 1–53.

Bottjer D. J., Davidson E. H. and Peterson K. J. (2006) Paleogenomics of echinoderms. *Science*.

Brand W. A., Assonov S. S. and Coplen T. B. (2010) Correction for the ^{17}O interference in δ (^{13}C) measurements when analyzing CO_2 with stable isotope mass spectrometry (IUPAC Technical Report). *Pure Appl. Chem.*.

Came R. E., Brand U. and Affek H. P. (2014) Clumped isotope signatures in modern brachiopod carbonate. *Chem. Geol.* **377**, 20–30.

Came R. E., Eiler J. M., Veizer J., Azmy K., Brand U. and Weidman C. R. (2007) Coupling of surface temperatures and atmospheric CO_2 concentrations during the Palaeozoic era. *Nature* **449**, 198–201.

Chave K. E. (1954) Aspects of the biogeochemistry of magnesium 1. Calcareous marine organisms. *J. Geol.* **62**, 266–283.

Clarke F. W. and Wheeler W. C. (1917) *The Inorganic Constituents of Marine Invertebrates*. Washington Government Printing Office, Washington.

Cleary D. F. R., Becking L. E., de Voogd N. J., Renema W., de Beer M., van Soest R. W. M. and Hoeksema B. W. (2005) Variation in the diversity and composition of benthic taxa as a function of distance offshore, depth and exposure in the Spermonde Archipelago, Indonesia. *Estuar. Coast. Shelf Sci.* **65**, 557–570.

Cohen J. (1992) A Power Primer. *Psycological Bulletin.* **122**, 122–155.

Coplen T. B. (1988) Normalization of oxygen and hydrogen isotope data. *Chem. Geol. (Isotope Geoscience Section)* **72**, 293–297.

Courtney T. and Ries J. B. (2015) Impact of atmospheric pCO_2, seawater temperature, and calcification rate on the δO and $\delta^{13}C$ composition of echinoid calcite (Echinometra viridis). *Chem. Geol.* **411**, 228–239.

Daëron M., Blamart D., Peral M. and Affek H. P. (2016) Absolute isotopic abundance ratios and the accuracy of Δ_{47} measurements. *Chem. Geol.*, 1–38.

Davies A. J. and John C. M. (2017) Reducing contamination parameters for clumped isotope analysis: the effect of lowering Porapak™ Q trap temperature to below 50 °C. *Rapid Commun. Mass Spectrom.* **31**, 1313–1323.

Defliese W. F., Hren M. T. and Lohmann K. C. (2015) Compositional and temperature effects of phosphoric acid fractionation on Δ_{47} analysis and implications for discrepant calibrations. *Chem. Geol.* **396**, 51–60.

Dietzel M., Tang J., Leis A. and Köhler S. J. (2009) Oxygen isotopic fractionation during inorganic calcite precipitation - Effects of temperature, precipitation rate and pH. *Chem. Geol.* **268**, 107–115.

Dennis K. J. and Schrag D. P. (2010) Clumped isotope thermometry of carbonatites as an indicator of diagenetic alteration. *Geochim. Cosmochim. Acta* **74**, 4110–4122.

Dennis K. J., Affek H. P., Passey B. H., Schrag D. P. and Eiler J. M. (2011) Defining an absolute reference frame for "clumped" isotope studies of CO_2. *Geochim. Cosmochim. Acta* **75**, 7117–7131.

Dennis K. J., Cochran J. K., Landman N. H. and Schrag D. P. (2013) The climate of the Late Cretaceous New insights from the application of the carbonate clumped isotope thermometer to Western Interior Seaway macrofossil. *Earth Planet. Sci. Lett.* **362**, 51–65.

DePaolo D. J. (2011) Surface kinetic model for isotopic and trace element fractionation during precipitation of calcite from aqueous solutions. *Geochim. Cosmochim. Acta* **75**, 1039–1056.

Dickson J. A. D. (1995) Paleozoic Mg calcite preserved: Implications for the Carboniferous ocean. *Geology.* **23**(6), 535–538.

Dickson J. (2001) Diagenesis and crystal caskets: echinoderm Mg calcite transformation, Dry Canyon, New Mexico, USA. *J. Sediment. Res.*.

Eagle R. A., Schauble E. A., Tripati A. K., Tütken T., Hulbert R. C., Eiler J. M. and Thiemens M. H. (2010) Body temperatures of modern and extinct vertebrates from C–O bond abundances in bioapatite. *PNAS* **107**, 10377–10382.

Eiler J. M. (2011) Paleoclimate reconstruction using carbonate clumped isotope thermometry. *Quat. Sci. Rev.* **30**, 3575–3588.

Eiler J. M. (2007) "Clumped-isotope" geochemistry—the study of naturally-occurring, multiply-substituted isotopologues. *Earth Planet. Sci. Lett.* **262**, 309–327.

Eiler J. M. and Schauble E. (2004) OCO in Earth's atmosphere. *Geochim. Cosmochim. Acta* **68**, 4767–4777.

Emiliani C. (1955) Pleistocene temperatures. *J. Geol.*.

Epstein S., Buchsbaum R., Lowenstam H. and Urey H. C. (1951) Carbonate-water isotopic temperature scale. *Geol. Soc. Am. Bull.* **62**, 417–426.

Evans D., Sagoo N., Renema W., Cotton L. J., Müller W., Todd J. A., Saraswati P. K., Stassen P., Ziegler M., Pearson P. N., Valdes P. J. and Affek H. P. (2018) Eocene greenhouse climate revealed by coupled clumped isotope-Mg/Ca thermometry. *Proc. Natl. Acad. Sci.* **115**, 1174–1179.

Faul F., Erdfelder E., Lang A.-G. and Buchner A. (2007) G*Power 3: a flexible statistical power analysis program for the social, behavioral, and biomedical sciences. *Behav. Res. Meth.* **39**, 175–191.

Gabitov R. I. (2013) Growth-rate induced disequilibrium of oxygen isotopes in aragonite: an in situ study. *Chem. Geol.* **351**, 268–275.

Ghosh P., Adkins J., Affek H., Balta B., Guo W., Schauble E. A., Schrag D. and Eiler J. M. (2006) C–O bonds in carbonate minerals: a new kind of paleothermometer. *Geochim. Cosmochim. Acta* **70**, 1439–1456.

Ghosh P., Eiler J., Campana S. E. and Feeney R. F. (2007) Calibration of the carbonate "clumped isotope" paleothermometer for otoliths. *Geochim. Cosmochim. Acta* **71**, 2736–2744.

Gorzelak P., Stolarski J., Dubois P., Kopp C. and Meibom A. (2011) 26 Mg labeling of the sea urchin regenerating spine: Insights into echinoderm biomineralization process. *J. Struct. Biol.* **176**, 119–126.

Grauel A.-L., Schmid T. W., Hu B., Bergami C., Capotondi L., Zhou L. and Bernasconi S. M. (2013) Calibration and application of the "clumped isotope" thermometer to foraminifera for high-resolution climate reconstructions. *Geochim. Cosmochim. Acta* **108**, 125–140.

Guo W., Daëron M., Niles P. and Genty D. (2008) ^{13}C–^{18}O bonds in dissolved inorganic carbon: implications for carbonate clumped isotope thermometry. *Geochimica et Cosmochimica Acta* **72**, A287–A338.

Guo W., Mosenfelder J. L., Goddard, III, W. A. and Eiler J. M. (2009) Isotopic fractionations associated with phosphoric acid digestion of carbonate minerals: insights from first-principles theoretical modeling and clumped isotope measurements. *Geochimica et Cosmochimica Acta* **73**, 7203–7225.

Henkes G. A., Passey B. H., Wanamaker, Jr, A. D., Grossman, Jr, E. L., Ambrose W. G. and Carroll M. L. (2013) Carbonate clumped isotope compositions of modern marine mollusk and brachiopod shells. *Geochim. Cosmochim. Acta* **106**, 307–325.

Hill P. S., Tripati A. K. and Schauble E. A. (2014) Theoretical constraints on the effects of pH, salinity, and temperature on clumped isotope signatures of dissolved inorganic carbon species and precipitating carbonate minerals. *Geochim. Cosmochim. Acta* **125**, 610–652.

Holcomb M., Venn A. A., Tambutté E., Tambutté S., Allemand D., Trotter J. and McCulloch M. (2014) Coral calcifying fluid pH dictates response to ocean acidification. *Sci. Rep.* **4**, 1–4.

John C. M. and Bowen D. (2016) Community software for challenging isotope analysis: first applications of "Easotope" to clumped isotopes. *Rapid Commun. Mass Spectrom.* **30**, 2285–2300.

Johnson K. S. (1982) Carbon dioxide hydration and dehydration kinetics in seawater1. *Limnol. Oceanogr.* **27**, 849–855.

Katz A., Bonifacie M., Hermoso M., Cartigny P. and Calmels D. (2017) Laboratory-grown coccoliths exhibit no vital effect in clumped isotope Δ_{47} composition on a range of geologically relevant temperatures. *Geochim. Cosmochim. Acta* **208**, 335–353.

Kelson J. R., Huntington K. W., Schauer A. J., Saenger C. and Lechler A. R. (2017) Toward a universal carbonate clumped isotope calibration: diverse synthesis and preparatory methods suggest a single temperature relationship. *Geochim. Cosmochim. Acta* **197**, 104–131.

Kim S.-T., Mucci A. and Taylor B. E. (2007) Phosphoric acid fractionation factors for calcite and aragonite between 25 and 75 °C: Revisited. *Chem. Geol.* **246**, 135–146.

Kimball J., Tripati R. E. and Dunbar R. (2015) Carbonate "clumped" isotope signatures in aragonitic scleractinian and calcitic gorgonian deep-sea corals. *Biogeosci. Discuss.* **12**, 19115–19165.

Kluge T., John C. M., Jourdan A.-L., Davis S. and Crawshaw J. (2015) Laboratory calibration of the calcium carbonate clumped isotope thermometer in the 25–250 °C temperature range. *Geochim. Cosmochim. Acta* **157**, 213–227.

Kroh A. and Nebelsick J. H. (2009) Echinoderms and Oligo-Miocene carbonate systems: potential applications in sedimentology and environmental reconstruction. *Int. Assoc. Sediment. Spec. Publ.* **42**, 201–226.

Lebrato M., Iglesias-Rodríguez D., Feely R. A., Greeley D., Jones D. O. B., Suarez-Bosche N., Lampitt R. S., Cartes J. E., Green D. R. H. and Alker B. (2010) Global contribution of echinoderms to the marine carbon cycle: $CaCO_3$ budget and benthic compartments. *Ecol. Monogr.* **80**, 441–467.

Lebeau O., Busigny V., Chaduteau C. and Ader M. (2014) Organic matter removal for the analysis of carbon and oxygen isotope compositions of siderite. *Chem. Geol.* **372**, 1–8.

LeGrande A. N. and Schmidt G. A. (2006) Global gridded data set of the oxygen isotopic composition in seawater. *Geophys. Res. Lett.* **33**, 15833–15835.

Locarnini, R.A., Mishonov, A.V., Antonov, J.I., 2013. World Ocean Atlas 2013, vol. 1, Temperature. NOAA Atlas NESDIS 73.

Marion G. M., Millero F. J., Camões M. F., Spitzer P., Feistel R. and Chen C. T. A. (2011) pH of Seawater. *Mar. Chem.* **126**, 89–96.

Markel K., Roser U., Mackenstedt U. and Klostermann M. (1986) Ultrastructural investigation of matrix-mediated biomineralization in echinoids (Echinodermata, Echinoida). *Zoomorphology*.

Mavromatis V., Schmidt M., Botz R., Comas-Bru L. and Oelkers E. H. (2012) Experimental quantification of the effect of Mg on calcite–aqueous fluid oxygen isotope fractionation. *Chem. Geol.* **310–311**, 97–105.

McClintock J. B., Amsler M. O., Angus R. A., Challener R. C., Schram J. B., Amsler C. D., Mah C. L., Cuce J. and Baker B. J. (2011) The Mg-calcite composition of antarctic echinoderms: important implications for predicting the impacts of ocean acidification. *J. Geol.* **119**, 457–466.

McConnaughey T. (1989a) ^{13}C and ^{18}O isotopic disequilibrium in biological carbonates: I. Patterns. *Geochimica et Cosmochimica Acta* **53**, 151–162.

McConnaughey T. (1989b) C and O isotopic disequilibrium in biological carbonates: II. In vitro simulation of kinetic isotope effects. *Geochim. Cosmochim. Acta* **53**, 163–171.

McCrea J. M. (1950) On the isotopic chemistry of carbonates and a paleotemperature scale. *J. Chem. Phys.* **18**, 849.

McCulloch M., Falter J., Trotter J. and Montagna P. (2012) Coral resilience to ocean acidification and global warming through pH up-regulation. *Nat. Clim. Change* **2**, 1–5.

Merrill R. J. and Hobson E. S. (1970) Field observations of dendraster-excentricus, a sand dollar of Western North-America. *Am. Midl. Nat.* **83**, 595-&.

Millero F. J., Graham T. B., Huang F., Bustos-Serrano H. and Pierrot D. (2006) Dissociation constants of carbonic acid in seawater as a function of salinity and temperature. *Mar. Chem.* **100**, 80–94.

Nebelsick J. H. and Kroh A. (2002) The stormy path from life to death assemblages: the formation and preservation of mass accumulations of fossil sand dollars. *Palaios* **17**, 378–393.

Passey B. H. and Henkes G. A. (2012) Carbonate clumped isotope bond reordering and geospeedometry. *Earth Planet. Sci. Lett.* **351–352**, 223–236.

Politi Y., Arad T., Klein E., Weiner S. and Addadi L. (2004) Sea urchin spine calcite forms via a transient amorphous calcium carbonate phase. *Science* **306**, 1161–1164.

Raz S., Hamilton P. C., Wilt F. H., Weiner S. and Addadi L. (2003) The transient phase of amorphous calcium carbonate in sea urchin larval spicules: the involvement of proteins and magnesium ions in its formation and stabilization. *Adv. Funct. Mater.* **13**, 480–486.

Richardson J. T. E. (2011) Eta squared and partial eta squared as measures of effect size in educational research. *Educ. Res. Rev.* **6**, 135–147.

Ries J. B. (2011) A physicochemical framework for interpreting the biological calcification response to CO_2-induced ocean acidification. *Geochim. Cosmochim. Acta* **75**, 4053–4064.

Ristanto A., Yanti A. H. and Setyawati T. R. (2018) Sea urchin (Echinoidea) distribution and abundance in the intertidal zone of Bengkayang regency. *J. Bio. Bio. Edu.* **10**, 32–40.

Saenger C., Affek H. P., Felis T., Thiagarajan N., Lough J. M. and Holcomb M. (2012) Carbonate clumped isotope variability in shallow water corals: temperature dependence and growth-related vital effects. *Geochim. Cosmochim. Acta* **99**, 224–242.

Schauble E. A., Ghosh P. and Eiler J. M. (2006) Preferential formation of C–O bonds in carbonate minerals, estimated using first-principles lattice dynamics. *Geochim. Cosmochim. Acta* **70**, 2510–2529.

Schauer A. J., Kelson J., Saenger C. and Huntington K. W. (2016) Choice of ^{17}O correction affects clumped isotope (Δ_{47}) values of CO_2 measured with mass spectrometry. *Rapid Commun. Mass Spectrom.* **30**, 2607–2616.

Schroeder J. H., Dwornik E. J. and Papike J. J. (1969) Primary protodolomite in echinoid skeletons. *Geol. Soc. Am. Bull.* **80**, 1613–1615.

Spooner P. T., Guo W., Robinson L. F., Thiagarajan N., Hendry K. R., Rosenheim B. E. and Leng M. J. (2016) Clumped isotope composition of cold-water corals: a role for vital effects? *Geochim. Cosmochim. Acta* **179**, 123–141.

Stumpp M., Hu M. Y., Melzner F., Gutowska M. A., Dorey N., Himmerkus N., Holtmann W. C., Dupont S. T., Thorndyke M. C. and Bleich M. (2012) Acidified seawater impacts sea urchin larvae pH regulatory systems relevant for calcification. *P. Natl. Ac. Sci. United States of America* **109**, 18192–18197.

Sutton J. N., Liu Y. W., Ries J. B. and Guillermic M. (2017) δ11B as monitor of calcification site pH in marine calcifyingorganisms. *Biogeosciences*.

Swart P. K., Burns S. J. and Leder J. J. (1991) Fractionation of the stable isotopes of oxygen and carbon in carbon dioxide during the reaction of calcite with phosphoric acid as a function of temperature and technique. *Chem. Geol. (Isotope Geosci. Sect.)*.

Tang J., Dietzel M., Fernandez A., Tripati A. K. and Rosenheim B. E. (2014) Evaluation of kinetic effects on clumped isotope fractionation Δ_{47} during inorganic calcite precipitation. *Geochim. Cosmochim. Acta* **134**, 120–136.

Thiagarajan N., Adkins J. and Eiler J. (2011) Carbonate clumped isotope thermometry of deep-sea corals and implications for vital effects. *Geochim. Cosmochim. Acta* **75**, 4416–4425.

Tripati A. K., Eagle R. A., Thiagarajan N., Gagnon A. C., Bauch H., Halloran P. R. and Eiler J. M. (2010) C–O isotope signatures and "clumped isotope" thermometry in foraminifera and coccoliths. *Geochim. Cosmochim. Acta* **74**, 5697–5717.

Tripati A. K., Hill P. S., Eagle R. A., Mosenfelder J. L., Tang J., Schauble E. A., Eiler J. M., Zeebe R. E., Uchikawa J., Coplen T. B., Ries J. B. and Henry D. (2015) Beyond temperature: clumped isotope signatures in dissolved inorganic carbon species and the influence of solution chemistry on carbonate mineral composition. *Geochim. Cosmochim. Acta* **166**, 344–371.

Wang D., Wallace A. F., De Yoreo J. J., Dove P. M. and Stanley S. M. (2009) Carboxylated Molecules Regulate Magnesium Content of Amorphous Calcium Carbonates during Calcification. *P. Natl. Ac. Sci. United States of America* **106**, 21511–21516.

Urey H. C. (1947) The thermodynamic properties of isotopic substances. *J. Chem. Soc. (Resumed)*.

Watkins J. M. and Hunt J. D. (2015) A process-based model for non-equilibrium clumped isotope effects in carbonates. *Earth Planet. Sci. Lett.* **432**, 152–165.

Watson E. B. (2004) A conceptual model for near-surface kinetic controls on the trace-element and stable isotope composition of abiogenic calcite crystals. *Geochim. Cosmochim. Acta* **68**, 1473–1488.

Watson E. B. and Liang Ya (1995) A simple model for sector zoning in slowly grown crystals: implications for growth rate and lattice diffusion, with emphasis on accessory minerals in crustal rocks. *Am. Mineral.* **80**, 1179–1187.

Weber J. N. (1968) Fractionation of the stable isotopes of carbon and oxygen in calcareous marine invertebrates—the Asteroidea, Ophiuroidea and Crinoidea. *Geochim. Cosmochim. Acta* **32**, 33–70.

Weber J. N. (1969) The incorporation of magnesium into the skeletal calcites of echinoderms. *Am. J. Sci.* **267**, 537–566.

Weber J. N. and Raup D. M. (1966a) Fractionation of the stable isotopes of carbon and oxygen in marine calcareous organisms—the Echinoidea. Part I. Variation of C^{13} and O^{18} content within indiduals. *Geochim. Cosmochim. Acta* **30**, 681–703.

Weber J. N. and Raup D. M. (1966b) Fractionation of the stable isotopes of carbon and oxygen in marine calcareous organisms—the Echinoidea. Part II. Environmental and genetic factors. *Geochim. Cosmochim. Acta* **30**, 705–736.

Weiss I. M., Tuross N., Addadi L. and Weiner S. (2002) Mollusc larval shell formation: amorphous calcium carbonate is a precursor phase for aragonite. *J. Exp. Zool.* **293**, 478–491.

Wilt F. H. (2002) Biomineralization of the Spicules of Sea Urchin Embryos. *Zoolog. Sci.* **19**, 253–261.

Zaarur S., Affek H. P. and Brandon M. T. (2013) A revised calibration of the clumped isotope thermometer. *Earth Planet. Sci. Lett.* **382**, 47–57.

Zeebe, R.E., Wolf-Gladrow, D.A., 2001. CO2 in Seawater: Equilibrium, Kinetics, Isotopes.

Associate editor: F. McDermott